

## Interatomic Coulombic decay following resonant core excitation of Ar in argon dimer

T. Miteva, Y.-C. Chiang, P. Koloren, A. I. Kuleff, K. Gokhberg, and L. S. Cederbaum

Citation: *The Journal of Chemical Physics* **141**, 064307 (2014); doi: 10.1063/1.4891986

View online: <http://dx.doi.org/10.1063/1.4891986>

View Table of Contents: <http://scitation.aip.org/content/aip/journal/jcp/141/6?ver=pdfcov>

Published by the [AIP Publishing](#)

---

### Articles you may be interested in

[Ab initio interatomic decay widths of excited states by applying Stieltjes imaging to Lanczos pseudospectra](#)  
J. Chem. Phys. **134**, 094107 (2011); 10.1063/1.3558739

[Nuclear motion in carbonyl sulfide induced by resonant core electron excitation](#)  
J. Chem. Phys. **133**, 144314 (2010); 10.1063/1.3502116

[Interatomic Coulombic decay and its dynamics in NeAr following K - L L Auger transition in the Ne atom](#)  
J. Chem. Phys. **131**, 104303 (2009); 10.1063/1.3211114

[On the interatomic electronic processes following Auger decay in neon dimer](#)  
J. Chem. Phys. **129**, 074307 (2008); 10.1063/1.2960593

[Isonuclear Trends of Resonant Transfer and LShell Excitation for the Collision of Ar \(8+, 11+, 13+\) Ions with 2/He Targets](#)  
AIP Conf. Proc. **748**, 118 (2005); 10.1063/1.1896482

---



**AIP** | Journal of  
Applied Physics

*Journal of Applied Physics* is pleased to  
announce **André Anders** as its new Editor-in-Chief

# Interatomic Coulombic decay following resonant core excitation of Ar in argon dimer

T. Miteva,<sup>1</sup> Y.-C. Chiang,<sup>1</sup> P. Kolorenč,<sup>2</sup> A. I. Kuleff,<sup>1</sup> K. Gokhberg,<sup>1,a)</sup>  
 and L. S. Cederbaum<sup>1</sup>

<sup>1</sup>*Theoretische Chemie, Physikalisch-Chemisches Institut, Universität Heidelberg, Im Neuenheimer Feld 229, D-69120 Heidelberg, Germany*

<sup>2</sup>*Institute of Theoretical Physics, Faculty of Mathematics and Physics, Charles University in Prague, V Holešovičkách 2, 180 00 Prague, Czech Republic*

(Received 6 June 2014; accepted 22 July 2014; published online 12 August 2014)

A scheme utilizing excitation of core electrons followed by the resonant-Auger – interatomic Coulombic decay (RA-ICD) cascade was recently proposed as a means of controlling the generation site and energies of slow ICD electrons. This control mechanism was verified in a series of experiments in rare gas dimers. In this article, we present fully *ab initio* computed ICD electron and kinetic energy release spectra produced following  $2p_{3/2} \rightarrow 4s$ ,  $2p_{1/2} \rightarrow 4s$ , and  $2p_{3/2} \rightarrow 3d$  core excitations of Ar in Ar<sub>2</sub>. We demonstrate that the manifold of ICD states populated in the resonant Auger process comprises two groups. One consists of lower energy ionization satellites characterized by fast interatomic decay, while the other consists of slow decaying higher energy ionization satellites. We show that accurate description of nuclear dynamics in the latter ICD states is crucial for obtaining theoretical electron and kinetic energy release spectra in good agreement with the experiment.

© 2014 AIP Publishing LLC. [<http://dx.doi.org/10.1063/1.4891986>]

## I. INTRODUCTION

Propagation of ionizing radiation through weakly bound media such as water solutions or rare gas matrices leads predominantly to ionization of the constituent atoms and molecules.<sup>1</sup> Electronically excited ions produced in the radiation track relax in fast intramolecular or intermolecular processes. Autoionization, photon emission, and dissociation are examples of the former, while charge transfer, interatomic Coulombic decay (ICD),<sup>2</sup> and related processes<sup>3</sup> are the examples of the latter pathways. Relaxation of the excited ions produces reactive species such as radicals and free electrons. The nature, quantities, and spatial distribution of these reactive species define chemical reactions taking place after the fast physico-chemical stage ( $\sim 1$  ps) is over.<sup>1</sup>

ICD, whereby an excited ion relaxes by ionizing a neighbor, has a special importance for generating chemically active species. It is highly efficient, especially when the excited moiety has many neighbors. ICD lifetimes of excited states in hydrated metal ions were found to be only a few fs,<sup>4</sup> i.e. comparable to the rates of intra-atomic Auger processes. Moreover, at each ICD step a free electron, as well as a radical, is produced<sup>5</sup> in addition to the originally ionized atom or molecule.

One of the intriguing questions about the ICD process is whether one can exercise control over its course, therefore, possibly influencing chemical reactions initiated by radiation. It has been demonstrated on the example of small ammonia clusters that by varying the pH of the medium one can switch ICD on and off.<sup>6</sup> Another scheme envisioning more

varied control of ICD was recently proposed and discussed in Ref. 7. It is based on the resonant-Auger – ICD (RA-ICD) cascade and utilizes remarkable properties of the resonant core excitation process to achieve control over both the location of ICD and the energy of the ICD electrons (see Fig. 1). At first, the system is irradiated by synchrotron light of suitable frequency leading to resonant excitation of a core electron of some atom or molecule to an unoccupied orbital. Such core excited states decay locally in a resonant Auger process<sup>8</sup> emitting a fast Auger electron and predominantly producing ionization satellites,<sup>9,10</sup> i.e. states of two-hole-one-particle (2h1p) character. These states are mostly located on an atom or molecule where the initial core excitation was produced.<sup>11</sup> They may further decay by ICD with neighboring species resulting in the emission of slow secondary electrons. As a result, two cations are formed in close proximity to each other which leads to a Coulomb explosion.

The resonant excitation of core electrons is a very sensitive probe of local electronic properties as evidenced by selective excitation of electrons localized on identical atoms placed in different chemical environment.<sup>12</sup> Hence, the photon energy deposition and the following ICD step happen at a specified location. Moreover, since the excitation proceeds resonantly, by tuning the incident photon energy a core electron can be controllably promoted to different virtual orbitals. This will result in the population of different satellite states in the resonant Auger process, and their subsequent interatomic decay will lead to different distributions of ICD electrons.

This RA-ICD cascade has been originally experimentally demonstrated in the nitrogen and carbon monoxide dimers following core excitation at the oxygen and nitrogen K-edges,<sup>13</sup> and in Ar<sub>2</sub> following excitation from the

<sup>a)</sup>Electronic mail: kirill.gokhberg@pci.uni-heidelberg.de

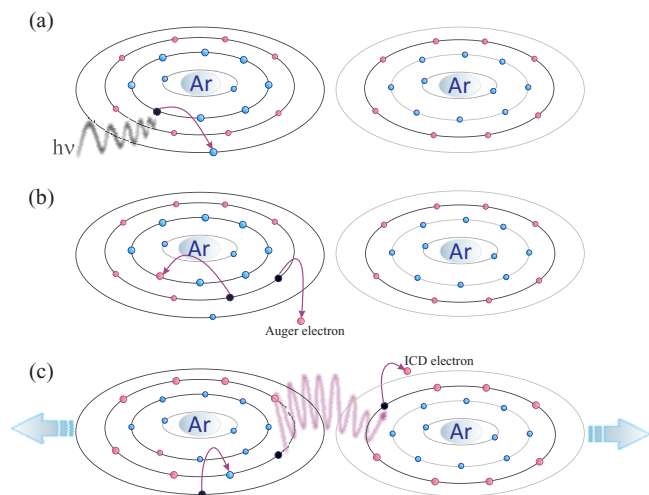


FIG. 1. Schematic representation of the resonant-Auger – ICD decay cascade: (a) resonant core excitation of Ar, resulting in the population of  $\text{Ar}(2p^{-1}nl)\text{Ar}$  state; (b) subsequent resonant Auger decay proceeding mostly according to the spectator model<sup>9</sup> in which the excited electron does not participate in the decay process. The excited electron can also hop to a higher virtual orbital (shake-up process). The final states are ionized-excited states of two-hole-one-particle (2h1p) character:  $\text{Ar}(3p^{-2}n'l)\text{Ar}$ . (c) The majority of the final states of the resonant Auger process undergo interatomic Coulombic decay, in which the excited electron de-excites and the excess energy is transferred to the neighbor, thus ionizing it. The final states of the ICD process are two-site dicationic states  $\text{Ar}^+(3p^{-1})\text{Ar}^+(3p^{-1})$ . Due to the repulsion between the charges, the system fragments in a Coulomb explosion.

$2p$  level.<sup>14</sup> Its detailed experimental studies in  $\text{Ar}_2$ ,  $\text{ArKr}$ ,  $\text{ArXe}$ , and  $\text{ArNe}$  demonstrated the functioning of the control mechanism.<sup>14–16</sup> In these experiments, the cascade was initiated by resonant photon excitation of a  $2p$  core electron of Ar to the  $4s$  or the  $nd$ ,  $n = 3, 4, 5$ , virtual orbital. Resulting ICD electron spectra indeed show marked dependence on the parent core excitation. For example, the spectra obtained in  $\text{Ar}_2$ ,  $\text{ArKr}$ , and  $\text{ArXe}$  following  $2p_{3/2} \rightarrow 4s$  excitation show a pronounced peak between 0 and 2 eV and a weaker peak between 2.5 and 4 eV, while the spectra obtained following  $2p_{3/2} \rightarrow 3d$  excitation have a characteristic double-peak structure shifted to higher energies.<sup>16</sup> The difference is due to the larger probability of shake-up processes in the resonant Auger decay of the  $2p_{3/2} \rightarrow 3d$  excitation on Ar.<sup>9,17,18</sup> This leads to a noticeable population (up to 60%) of higher lying  $\text{Ar}^+(3p^{-2}4d, 5d)$  satellite states.

The distribution of ICD electron energies can be qualitatively obtained using a simple model, where one assumes no interaction between atoms in the satellite states, pure Coulomb repulsion in the final states, and instantaneous decay.<sup>7</sup> Therefore, only readily available energies of different states of  $\text{Ar}^+$  and the ground state equilibrium distance of the corresponding dimer are necessary for computing ICD spectra. However, in  $\text{Ar}_2$  such qualitative approach overestimates the energies of ICD electrons deriving from the decay of higher-lying satellites.<sup>15</sup> Moreover, the observed kinetic energy release (KER) spectra show a complicated structure indicative of nuclear dynamics taking place during the decay. Thus, if one wishes to achieve a more detailed understanding of the resonant-Auger – ICD cascade, both accurate potential

energy curves (PECs) and accounting for the nuclear motion are indispensable.

In this article, we investigate the ICD process in  $\text{Ar}_2$  following the resonant Auger decay of  $2p_{3/2} \rightarrow 4s$ ,  $2p_{1/2} \rightarrow 4s$ , and  $2p_{3/2} \rightarrow 3d$  core excitations on Ar. The major goal is to study what role the accurate interaction energies in the decaying and final states of ICD and the nuclear dynamics during the decay play in shaping the ICD electron and KER spectra. We assume that the cascade is initiated by a broad resonant excitation so that the ground state wave packet is transferred vertically to the PEC of the specific  $2p \rightarrow nl$  core excited state of Ar. The lifetime of these states is  $\sim 6$  fs<sup>19</sup> and, therefore, the resonant Auger decay will be nearly unaffected by the nuclear dynamics on the core-excited PEC. Due to these assumptions of instantaneous core excitation and resonant Auger decay, the nuclear dynamics of the whole cascade is restricted to the dynamics during the ICD process. For the full quantum mechanical simulation of the dynamics one requires accurate *ab initio* potential energy curves and ICD widths as the input.

The article is structured as follows. In Sec. II, we provide the details of the computations of the potential energy curves and the decay widths, as well as the description of the nuclear dynamics calculations. In Sec. III, we discuss the properties of the potential energy curves, the nuclear dynamics during the resonant-Auger – ICD cascade, and the final ICD electron and KER spectra. Section IV summarizes our findings. The conclusions are given in Sec. IV.

## II. COMPUTATIONAL DETAILS

### A. Potential energy curves

The ground state potential curve of  $\text{Ar}_2$  was obtained using the coupled cluster singles and doubles and perturbative triples method (CCSD(T)) as implemented in the GAMESS-US package.<sup>20,21</sup> The basis set used on Ar was aug-cc-pV6Z<sup>22</sup> and an additional set of diffuse basis functions was added at the midpoint position between the two atoms. The exponents of the latter functions were taken to be the most diffuse  $s$ ,  $p$ ,  $d$ ,  $f$ , and  $g$  exponents from the aug-cc-pV6Z basis set. The minimum and the binding energy of the computed ground state potential energy curve are  $R_e = 3.80$  Å and  $D_e = 11.5$  meV, respectively, which is in good agreement with the experimental values of 3.76 Å and 12.3 meV.<sup>23</sup>

The PECs of the ionized excited states were computed using the configuration interaction (CI) method as implemented in the GAMESS-US computational package.<sup>24,25</sup> The CI-expansion comprises all single and double excitations (CISD) from the reference configurations. The latter were constructed from all possible 1h-configurations in which the 8 valence orbitals of  $\text{Ar}_2$  (converging to the  $3s$  and  $3p$  atomic orbitals of Ar at asymptotic distances) were occupied with 15 electrons. The cc-pVDZ<sup>26</sup> basis set augmented with two diffuse  $s$  functions, two diffuse  $d$  functions and two compact  $d$  functions was used on Ar. The additional diffuse and compact basis functions were generated as an even-tempered sequence ( $\xi = \alpha\beta^l$ ) from the most diffuse  $s$  and  $d$  and the most compact  $d$  exponents, respectively, with  $\beta = 10$  and  $l = \pm 1/2$  ( $l = 1/2$  in

the case of the compact exponents, and  $-1/2$  for the diffuse exponents).<sup>27</sup>

The PECs of the low-lying members of the Rydberg series (namely, the  $\text{Ar}^+(3p^{-2}4s)\text{Ar}$  and  $\text{Ar}^+(3p^{-2}3d)\text{Ar}$  states) were found among the first 100 roots of the CI matrix in all irreducible representations of the  $D_{2h}$  point group. The PECs of the higher  $\text{Ar}^+(3p^{-2}5s)\text{Ar}$  satellites could also be distinguished among the first 100 excited states. However, obtaining the PECs of the  $\text{Ar}^+(3p^{-2}4d)\text{Ar}$  Rydberg states was beyond our reach. First, this task requires the computation of a very large number of roots. Second, due to the high density of states at higher energies the recovery of the corresponding PECs from the data becomes extremely difficult. An alternative approach to the straightforward computation of these states is to model them. We have shown<sup>28</sup> that the PECs of higher satellites at the interatomic distances where the nuclear dynamics predominantly takes place can be fairly accurately reproduced by the PECs of the corresponding parent dicationic states. Therefore, the PECs of the  $\text{Ar}^+(3p^{-2}4d)\text{Ar}$  states were approximated by averages of the PECs of the parent  $\text{Ar}^{++}(3p^{-2})\text{Ar}$  states.

The computation of the PECs of the final two-site dicationic states, as well as the one-site states used to approximate the higher-lying ionization satellites was carried out using the same implementation of the CISD method and basis set as for the singly ionized states. The reference space in this case comprises all possible 2h-configurations with 14 electrons occupying the 8 valence orbitals of  $\text{Ar}_2$  (the 3s and 3p orbitals of each Ar atom). Two sets of reference spaces were constructed corresponding to the two possible spin multiplicities (singlet and triplet).

At asymptotic distances the PECs of the ionization satellites and two-site dicationic final states were adjusted to the correct asymptotic energies taken from the NIST database.<sup>29</sup> The NIST energies were averaged over all possible fine-structure components since the spin-orbit coupling was not accounted for in our calculations.

## B. Decay widths

The ICD widths were computed using the Fano-Stieltjes method, with the bound and continuum part of the corresponding resonance state constructed using the extended ADC(2) scheme for the one-particle propagator.<sup>30</sup> For this purpose, we used on each atom an effective core potential (ECP) with 4s, 4p, 4d, and 1f basis functions with 8 active valence electrons. The ECP was adjusted in energy to non-relativistic and scalar relativistic energies.<sup>31</sup> The basis was further augmented by 8s, 8p, 8d, 5f, and 3g diffuse functions on the atomic centers and additional sets of 3s, 3p, and 4d functions on 5 ghost centers on the interatomic axis. The diffuse functions were specifically designed for the computation of Rydberg and continuum states.<sup>32</sup>

Characteristic rates of the ICD states at  $R_e$  and at left turning points of the respective PECs are listed in Table I. We would like to note that in contrast to the computation of PECs using the CISD method, in the Fano-Stieltjes method the higher-lying ionization satellites are still accessible. The

TABLE I. *Ab initio* decay widths of the ionization satellites of  $\text{Ar}_2$  accounted for in the nuclear dynamics calculations. The R-dependent decay widths enter both differential equations in Eq. (1) as the operators  $\hat{\Gamma}_i(R)$  and  $\hat{W}_{jk}^i(R)$ . Here we present the values of the decay widths only at the equilibrium interatomic distance  $R_e$  and at the left turning points  $R_{t.p.}$  of the ICD PECs. The states for which the value at  $R_{t.p.}$  is missing are dissociative. One can see that the decay widths of the low Rydberg states at  $R_e$  are by an order of magnitude higher than those of the high-lying Rydberg states. Thus, the decay of the low-lying ionization satellites is fast, taking place at  $R_e$ , whereas the decay of the high-lying ionization satellites is influenced by the nuclear motion and happens mainly in the vicinity of the left turning point  $R_{t.p.}$  of the corresponding potential curve, where the decay width is much higher.

$\text{Ar}^+\text{Ar}$ state	Term symbol	$\Gamma(R_e)$ , meV	$\Gamma(R_{t.p.})$ , meV
$3p^{-2} [^1S]4s^2S$	$\Sigma_g^+$	12.32	–
	$\Sigma_u^+$	12.83	–
$[^1D]3d^2D$	$\Sigma_g^+$	47.27	80.43 (3.39 Å)
	$\Sigma_u^+$	37.37	74.66 (3.25 Å)
	$\Pi_g^+$	28.91	39.57 (3.63 Å)
	$\Pi_u^+$	35.20	–
	$\Delta_g^+$	15.00	19.24 (3.20 Å)
	$\Delta_u^+$	13.88	9.04 (3.09 Å)
$[^1D]3d^2P$	$\Sigma_g^-$	11.63	–
	$\Sigma_u^-$	10.12	–
	$\Pi_g^-$	24.57	41.85 (3.12 Å)
	$\Pi_u^-$	28.13	–
$[^1S]3d^2D$	$\Sigma_g^+$	1.04	–
	$\Sigma_u^+$	0.97	–
	$\Pi_g^+$	1.19	14.51 (3.17 Å)
	$\Pi_u^+$	1.79	11.51 (3.23 Å)
	$\Delta_g^+$	4.36	23.60 (3.34 Å)
	$\Delta_u^+$	4.36	14.22 (3.48 Å)
$[^1D]5s^2D$	$\Sigma_g^+$	1.04	21.68 (2.85 Å)
	$\Sigma_u^+$	0.90	14.49 (2.82 Å)
	$\Pi_g^+$	0.33	5.89 (2.83 Å)
	$\Pi_u^+$	0.31	4.23 (2.92 Å)
	$\Delta_g^+$	0.68	5.49 (2.79 Å)
	$\Delta_u^+$	0.58	4.21 (2.78 Å)
$[^3P]5s^2P$	$\Sigma_g^-$	2.24	15.13 (2.91 Å)
	$\Sigma_u^-$	1.95	11.55 (2.90 Å)
	$\Pi_g^-$	0.76	20.02 (2.93 Å)
	$\Pi_u^-$	0.82	11.94 (2.98 Å)
	$\Delta_g^-$	0.83	20.70 (2.75 Å)
$[^1D]4d^2P$	$\Sigma_u^-$	0.73	13.26 (2.75 Å)
	$\Pi_g^-$	0.59	10.82 (2.77 Å)
$[^1D]4d^2D$	$\Pi_u^-$	0.63	15.83 (2.77 Å)
	$\Sigma_g^+$	1.22	14.23 (2.77 Å)
	$\Sigma_u^+$	0.85	7.84 (2.77 Å)
	$\Pi_g^+$	0.39	20.47 (2.77 Å)
	$\Pi_u^+$	0.43	20.50 (2.77 Å)
	$\Delta_g^+$	0.72	14.52 (2.77 Å)
$[^1D]4d^2F$	$\Delta_u^+$	0.70	13.54 (2.77 Å)
	$\Sigma_g^-$	0.37	10.34 (2.75 Å)
	$\Sigma_u^-$	0.36	11.84 (2.75 Å)
	$\Pi_g^-$	0.31	8.15 (2.77 Å)
	$\Pi_u^-$	0.30	7.76 (2.77 Å)
	$\Delta_g^-$	0.20	13.04 (2.77 Å)
	$\Delta_u^-$	0.22	12.92 (2.77 Å)
	$\Phi_g^+$	0.55	3.93 (2.75 Å)
$\Phi_u^+$	0.61	3.13 (2.75 Å)	

projection on the bound states subspace simplifies the ionization spectrum significantly, which facilitates the identification of the states in question. For the lowest Rydberg terms these widths vary between 47 and 1 meV corresponding to the lifetimes between 28 fs and 1.35 ps. For the higher states, the widths become considerably smaller and range between 2.2 and 0.2 meV corresponding to the lifetimes between 0.6 and 6.6 ps. Therefore, the ICD rate decreases with the increase of the principal quantum number  $n$  of the excited electron, which is expected as the Rydberg orbitals become more diffuse for larger  $n$ 's, resulting in a smaller overlap with the dicationic core and smaller ICD rates.<sup>2</sup> The widths also depend strongly on the interatomic distance  $R$  becoming larger as  $R$  decreases. At large  $R$  they behave as  $1/R^6$  and grow even faster about  $R_e$  due to the effect of orbital overlap.<sup>33</sup>

Within the present method partial decay widths, needed for the nuclear dynamics calculations, cannot be reliably computed. Instead, they were assumed to be equal and were obtained by dividing the total decay width of the  $i$ th ICD state by the number of channels, i.e.  $\Gamma_{f_k}^i(R) = \Gamma_i(R)/N_c$ . In the case of Ar<sub>2</sub>, there are 18 decay channels.

### C. Nuclear dynamics calculations

As we already mentioned, under the assumption of an instantaneous core excitation and a very fast resonant Auger step, significant nuclear dynamics only take place during the ICD step of the cascade. The nuclear dynamics during the ICD step can be described by the wave packets propagating on the PECs of the decaying and final states. Similar to the previous calculations of ICD dynamics,<sup>34–37</sup> we neglected the interactions among the decaying and final states. Consequently, the equations of motion describing the time-evolution of the nuclear wave packets read<sup>38</sup>

$$\begin{aligned} i|\dot{\Psi}_{d_i}(t)\rangle &= (\hat{H}_{d_i} - i\hat{\Gamma}_i(R)/2)|\Psi_{d_i}(t)\rangle, \\ i|\dot{\Psi}_{f_k}^i(E_e, t)\rangle &= (\hat{H}_{f_k} + E_e)|\Psi_{f_k}^i(E_e, t)\rangle + \hat{W}_{f_k}^i(R)|\Psi_{d_i}(t)\rangle, \end{aligned} \quad (1)$$

where  $\hat{H}_{d_i}$  and  $\hat{H}_{f_k}$  are the Hamiltonians for the nuclear motion in the decaying and final states, respectively, while  $|\Psi_{d_i}(t)\rangle$  and  $|\Psi_{f_k}^i(E_e, t)\rangle$  denote the corresponding nuclear wave packets. Note that the final-state nuclear wave packet depends on the kinetic energy of the ICD electron ( $E_e$ ). The transition element  $\hat{W}_{f_k}^i(R)$  is related to the partial decay width of the state  $i$  into the state  $f_k$  as  $\hat{\Gamma}_i^i(R) = 2\pi|\hat{W}_{f_k}^i(R)|^2$  in the local approximation (see Refs. 38–41).

The time evolution of the nuclear wave packets was computed using the Lanczos-Arnoldi algorithm<sup>42</sup> as implemented in the multi-configuration time-dependent Hartree (MCTDH) package.<sup>43,44</sup> The computations were done for the internuclear distances between 1.50 Å and 11.73 Å using fast Fourier transform (FFT) with 1024 points. The nuclear wave packets of the decaying and final states were propagated until the norm of the wave function of the decaying state becomes of the order of  $10^{-8}$ . Depending on the ionization satellite the propagation times varied between 500 fs and 150 ps.

The kinetic energy distributions of the emitted electrons following the decay in a particular channel can be obtained from the nuclear wave packet on the corresponding final state at large times, when the decay is essentially complete<sup>38</sup>

$$\sigma_{f_k}^i(E_e) = \lim_{t \rightarrow \infty} \langle \Psi_{f_k}^i(E_e, t) | \Psi_{f_k}^i(E_e, t) \rangle. \quad (2)$$

The ICD electron spectrum of a particular decaying state is then the sum of the partial intensities  $\sigma_{f_k}^i(E_e)$ , which correspond to all possible decay channels:

$$\sigma_{ICD}^i(E_e) = \sum_k \sigma_{f_k}^i(E_e). \quad (3)$$

The kinetic energy release (KER) spectra of the nuclei following the decay from the state  $i$  were evaluated as

$$\sigma_{KER}^i(E_{KER}) = \sigma_{ICD}^i(E_i(R_e) - E_f(\infty) - E_e), \quad (4)$$

where  $E_{KER}$  is the kinetic energy of the nuclei,  $E_i(R_e)$  is the electronic energy of the decaying state at  $R_e$ ,  $E_f(\infty)$  is the asymptotic energy of the final states (the same for all 18 channels in our case). Although computing the KER spectrum via Eq. (4) is an approximation, known as the mirror image principle,<sup>45–47</sup> we found that it holds well in the case of Ar dimer. Note that the mirror image principle is invalid in the case of total ICD electron and KER spectra, which are obtained by summing the spectra of all decaying states.

The total ICD electron and KER spectra of a cascade initiated by a particular core excitation were calculated as weighted sums of the spectra belonging to the ionization satellites populated in the resonant Auger step. The respective weights for Ar<sub>2</sub> were obtained from the known branching ratios of this process in isolated Ar.<sup>18</sup> This assumption is confirmed by the experimental results reported in Ref. 14, which show that even in the dimer the resonant Auger decay is mostly of local nature. Finally, we convolve the total ICD electron and KER spectra with Gaussians of FWHM 1.24 eV and 0.64 eV, respectively, to account for the experimental resolution.<sup>14,16</sup>

## III. RESULTS AND DISCUSSION

### A. Potential energy curves

In the following, we will focus on the properties of the PECs of all states relevant for the nuclear dynamics, namely, the ground state of the neutral dimer Ar<sub>2</sub>, the ionization satellites Ar<sup>+</sup>(3p<sup>-2</sup>nl)Ar populated after the resonant Auger decay, and the final dicationic states of the ICD process Ar<sup>+</sup>(3p<sup>-1</sup>)Ar<sup>+</sup>(3p<sup>-1</sup>). These PECs are presented in Fig. 2. The potential curves of the core-excited states were not computed, since, as we mentioned in the Introduction, we assume that no significant nuclear dynamics take place during the RA process.

The ground state PEC of Ar<sub>2</sub> (see Fig. 3(a)) is characterized by a shallow minimum of  $D_e = 11.5$  meV located at  $R_e = 3.8$  Å. This potential supports seven vibrational levels. We assume that the argon dimer is in its lowest vibrational state which corresponds to the experimental conditions. Therefore, the initial wave packet is taken to be the respective nodeless

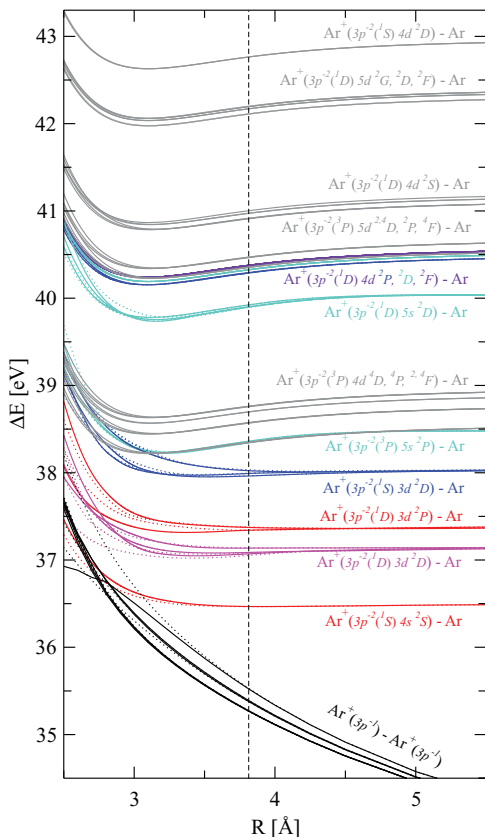


FIG. 2. Potential energy curves of the initial states populated in the resonant Auger decay of the core excitation of Ar in  $\text{Ar}_2$ , and the final states of the ICD process. The final repulsive two-site dicationic states  $\text{Ar}^+(3p^{-1})\text{Ar}^+(3p^{-1})$  are depicted as black curves. The low-lying ionization satellites in which ICD is faster than the nuclear vibrational motion are shown in red and pink. The higher-lying Rydberg states in which ICD is influenced by nuclear dynamics are presented as blue and violet curves (see Table I for the corresponding decay widths). The states populated in the resonant Auger step but not accounted for in the dynamics calculations are shown in grey.

eigenfunction of the nuclear Hamiltonian and has an approximately Gaussian shape.

The initial ICD states of interest are ionization satellites populated in the RA step. Due to a large number of such states,<sup>18</sup> it will be computationally prohibitive to take them all into account in calculating the ICD spectra. Therefore, we restrict the initial ICD states to include only the spin doublet satellites (see Table I for the corresponding states) originating from the states populated by more than 3% in the RA decay of isolated Ar (see Ref. 18 for the respective populations). These states form more than 60% of all states populated in the RA decay of the  $2p_{3/2} \rightarrow 3d$  core excitation that can further decay via ICD. This proportion rises to about 75% for the  $2p_{3/2, 1/2} \rightarrow 4s$  core excitations. As we will see, this selection is sufficient for accurately reproducing the experimental spectra. The PECs of these states are shown in Fig. 2.

One can better understand the structure of the ICD electron and KER spectra if the interatomic decay of the low- and high-lying Rydberg states populated in the RA step is considered separately. The former comprise the satellites correlating with the  $\text{Ar}^+(3p^{-2}[1S]4s^2S)\text{Ar}$ ,  $\text{Ar}^+(3p^{-2}[1D]3d^2D)\text{Ar}$ ,  $\text{Ar}^+(3p^{-2}[1D]3d^2P)\text{Ar}$ , and  $\text{Ar}^+(3p^{-2}[1S]3d^2D)\text{Ar}$  states at asymptotic distances. Their PECs possess shallow minima

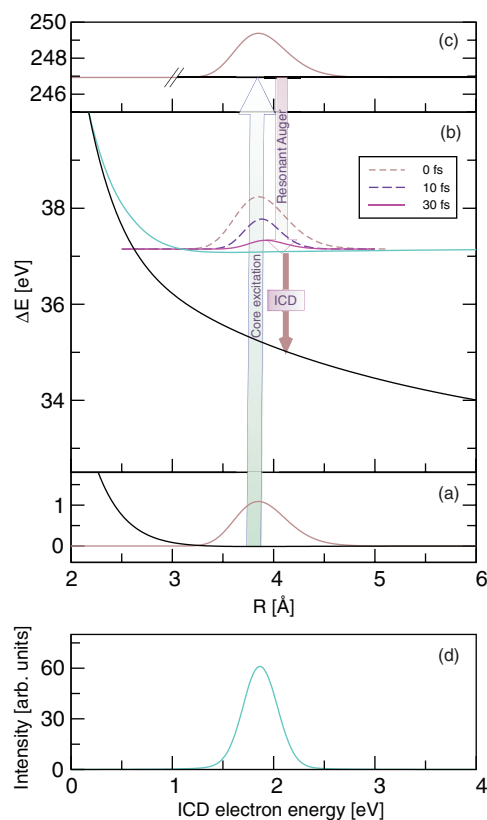


FIG. 3. Resonant-Auger - ICD cascade of the  $2p_{3/2} \rightarrow 3d$  excitation proceeding with a fast ICD step through the  $\text{Ar}^+(3p^{-2}[1D]3d^2D^2\Sigma_g^+)\text{Ar}$  satellite. The ground state PEC and the corresponding ground state nuclear wave packet density are depicted in panel (a). The cascade is initiated with a resonant core excitation of the initial wave packet to the  $\text{Ar}(2p_{3/2} \rightarrow 3d)\text{Ar}$  state (c) and subsequent instantaneous resonant Auger decay. Due to the very fast Auger step, the initial wave packet is vertically transformed to the potential surface of the  $\text{Ar}^+(3p^{-2}[1D]3d^2D^2\Sigma_g^+)\text{Ar}$  satellite (b) ( $t = 0$  fs). ICD follows resulting in the population of the  $\text{Ar}^+(3p^{-1})\text{Ar}^+(3p^{-1})^1\Delta_g$  final state, which is repulsive and the system fragments. The time-evolution of the nuclear wave packet of the decaying state shows that the shape of the initial wave packet is preserved due to the much faster decay as compared to the vibrational motion of the nuclei. Similarly to the Auger step, the wave packet is vertically transferred to the final state PEC. Therefore, the ICD electron spectrum (d) of the  $\text{Ar}^+(3p^{-2}[1D]3d^2D^2\Sigma_g^+)\text{Ar}$  state has a nearly Gaussian shape resembling that of the initial nuclear wave packet of the decaying state. The spectra of all fast decaying states have a similar nearly Gaussian shape (see Fig. 5).

located between 3.37 and 4.90 Å with interaction energies ranging between 36 and 129 meV. At the equilibrium distance, the ICD lifetimes of these states range between 28 and 130 fs being an order of magnitude smaller than the characteristic vibrational periods (0.6 ÷ 1.3 ps). Therefore, these intermediate states are expected to decay fast with little dynamics taking place during the decay. The PECs of the higher Rydberg states correlating with the  $\text{Ar}^+(3p^{-2}[3P]5s^2P)\text{Ar}$ ,  $\text{Ar}^+(3p^{-2}[1D]5s^2D)\text{Ar}$ ,  $\text{Ar}^+(3p^{-2}[1D]4d^2P, 2D, 2F)\text{Ar}$  satellites at asymptotic distances have somewhat different binding properties compared to the lower Rydberg states. These PECs are generally characterized with a deeper potential well, with binding energies between 250 meV and 340 meV, and minima shifted to shorter internuclear distances (3.08 ÷ 3.24 Å). This can be explained by smaller repulsion between the excited electron occupying a diffuse high Rydberg orbital and the

neutral Ar neighbor.<sup>28</sup> As a result, these states have smaller characteristic vibrational periods ( $180 \div 250$  fs). These, in turn, are by an order of magnitude shorter than the relevant ICD lifetimes at  $R_e$ . Therefore, the decay of these states is expected to be substantially influenced by the vibrational motion of the nuclei. The decay takes place mostly at shorter internuclear distances, where the respective width is an order of magnitude larger compared to its value at  $R_e$  (see Table I).

The final ICD states are presented in Fig. 2. There are 12 two-site final dicationic states of the  $\text{Ar}^+(3p^{-1})\text{Ar}^+(3p^{-1})$  with symmetries  $^1\Sigma_g^+(2)$ ,  $^3\Sigma_u^+(2)$ ,  $^1\Sigma_u^-$ ,  $^3\Sigma_g^-$ ,  $^1\Pi_g$ ,  $^3\Pi_g$ ,  $^1\Pi_u$ ,  $^3\Pi_u$ ,  $^1\Delta_g$ ,  $^3\Delta_u$ , resulting in 18 decay channels in total. Their PECs are all repulsive in the range of internuclear distances relevant for the decay, and behave as  $R^{-1}$  at large distances due to the dominant Coulomb repulsion between the two positively charged ions  $\text{Ar}^+$ . Therefore, ICD will be followed by a fast dissociation of the dimer.

## B. Nuclear dynamics during the ICD step

In order to obtain a clearer picture of the role nuclear dynamics play during the final ICD step, we will consider the fast and slow decaying ionization satellites separately. In Secs. II A and III A, we already defined two groups of states, namely, the low and high Rydberg states. The low Rydberg states  $\text{Ar}^+(3p^{-2}3d)\text{Ar}$  and  $\text{Ar}^+(3p^{-2}4s)\text{Ar}$  fall into the group of the fast decaying states, while the higher Rydberg states,  $\text{Ar}^+(3p^{-2}4d)\text{Ar}$  and  $\text{Ar}^+(3p^{-2}5s)\text{Ar}$ , are the slow decaying states. The ICD electron and KER spectra are profoundly different for these two groups. We demonstrate this difference by examining the ICD electron spectra of two specific satellites.

First, consider the decay cascade proceeding via the  $\text{Ar}^+(3p^{-2}[^1D]3d^2D^2\Sigma_g^+)\text{Ar}$  ionization satellite which is shown in Fig. 3. The PEC of this state is bound by 70 meV at 3.57 Å and supports 25 vibrational levels. At the equilibrium distance, the characteristic vibrational period is about 600 fs, which is an order of magnitude larger than the ICD lifetime of 28 fs. Therefore, the decay outpaces the vibrational motion and, thus, ICD occurs essentially at the internuclear separation at which the state was initially populated, i.e. at the equilibrium distance of the ground state. As one can see from the time evolution of the nuclear wave packet, presented in Fig. 3(b), its initial shape is not distorted by the vibrational motion, and the position of its maximum is also unaltered during the decay. The electron spectrum of this satellite is depicted in Fig. 3(d). It has a nearly Gaussian shape with a maximum at the electronic energy of 1.86 eV. It corresponds to the difference between the energy of the decaying state and that of the final electronic state at the equilibrium distance.

Let us focus next on the cascade proceeding via the  $\text{Ar}^+(3p^{-2}[^1D]5s^2D^2\Sigma_g^+)\text{Ar}$  satellite shown in Fig. 4. The PEC of this state possesses a deeper minimum of 307 meV located at 3.15 Å. It supports 39 vibrational levels and the characteristic time of vibrational motion was estimated to be about 200 fs. At  $R_e$  the ICD lifetime is 1270 fs, i.e. an order of magnitude larger than the vibrational period. As a result, after the state is populated, the wave packet at first becomes broader and shifts towards shorter internuclear dis-

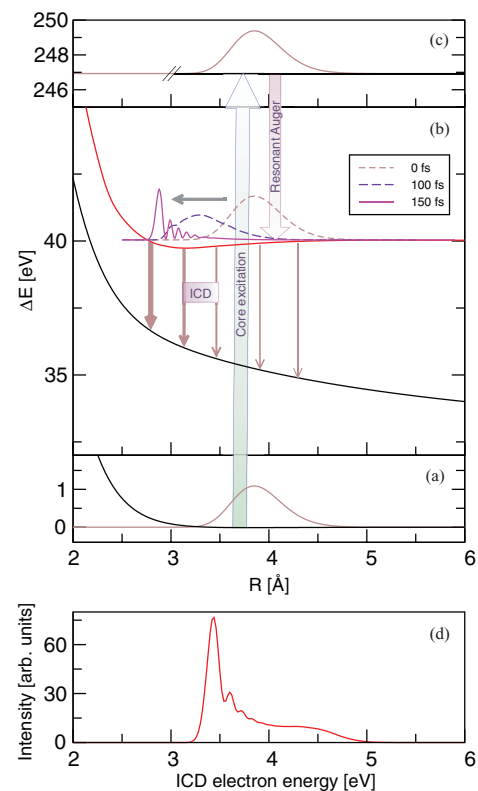


FIG. 4. Resonant-Auger - ICD cascade of the  $2p_{3/2} \rightarrow 3d$  excitation proceeding with a slow ICD step through the  $\text{Ar}^+(3p^{-2}[^1D]5s^2D^2\Sigma_g^+)\text{Ar}$  satellite. The ground state PEC and the corresponding ground state nuclear wave packet density are depicted in panel (a). The cascade is initiated with a resonant core excitation of the initial wave packet to the  $\text{Ar}(2p_{3/2} \rightarrow 3d)\text{Ar}$  state (c) and subsequent instantaneous resonant Auger decay. Due to the very fast Auger step, the initial wave packet is vertically transformed to the potential surface of the  $\text{Ar}^+(3p^{-2}[^1D]5s^2D^2\Sigma_g^+)\text{Ar}$  satellite (b) ( $t = 0$  fs). ICD follows resulting in the population of the  $\text{Ar}^+(3p^{-1})\text{Ar}^+(3p^{-1})\ ^1\Delta_g$  final state which is repulsive and the system fragments. The time-evolution of the nuclear wave packet of the decaying state shows the interplay between vibrational motion and decay. Due to the ICD lifetime being much longer than the characteristic vibrational period at the equilibrium distance, the initial wave packet starts moving towards shorter internuclear distances. The decay occurs mostly in the vicinity of the left turning point of the PEC. Therefore, the ICD electron spectrum of the  $\text{Ar}^+(3p^{-2}[^1D]5s^2D^2\Sigma_g^+)\text{Ar}$  state (d) has an irregular shape reflecting the competition between nuclear dynamics on the PEC of the ionization satellite and decay to the final two-site dicationic states. The spectra of all slow decaying states have a similar distorted shape (see Fig. 5).

At later times the wave packet acquires a characteristic multinodal structure with a dominant maximum located close to the left turning point (see Fig. 4(b)). Since the decay rate increases fast with the decreasing interatomic distance, ICD occurs mostly in the vicinity of the left turning point of the PEC, where the corresponding rate is approximately 20 times larger than at  $R_e$ . The resulting electron spectrum is shown in Fig. 4(d). The effect of nuclear dynamics on the spectrum is clearly visible in the dominant peak at 3.44 eV which corresponds to ICD taking place when the two argon atoms are approximately 2.9 Å apart, i.e. at the left turning point. The shoulder at 4.5 eV is a vestige of the decay which happened in the vicinity of  $R_e$ . Similar evolution of the vibrational wave during ICD was experimentally observed and

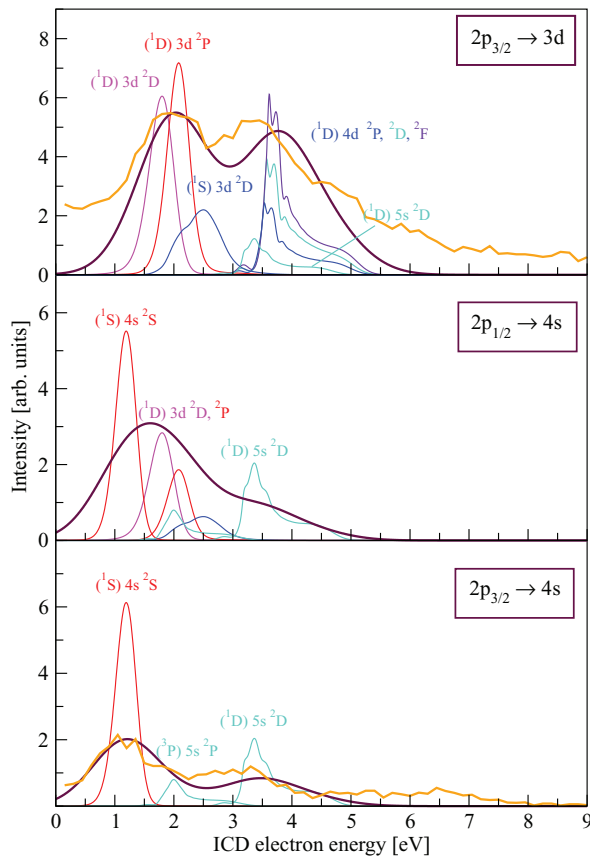


FIG. 5. ICD electron spectra obtained in the RA-ICD cascade following the  $\text{Ar}(2p_{3/2} \rightarrow 4s)\text{Ar}$  (lowermost panel),  $\text{Ar}(2p_{1/2} \rightarrow 4s)\text{Ar}$  (middle panel), and  $\text{Ar}(2p_{3/2} \rightarrow 3d)\text{Ar}$  (uppermost panel) core excitation. The dark red curves in all panels represent the total ICD spectra corresponding to the particular core excitation. Experimental data are available for the  $\text{Ar}(2p_{3/2} \rightarrow 4s)\text{Ar}$  and  $\text{Ar}(2p_{3/2} \rightarrow 3d)\text{Ar}$  excitation (orange curves).<sup>16</sup> In order to compare the experimental spectra with the theoretical ones, the latter were convolved using a Gaussian of FWHM 1.24 eV and scaled so that the intensities of the lower-energy peaks coincide. The electron spectra resulting from the decay of the individual satellites contributing to the total spectrum of each core excitation are also presented (the color scheme follows that of the PECs in Fig. 2).

confirmed numerically for the slow decaying satellite states of the He dimer.<sup>48,49</sup>

The states converging to  $\text{Ar}^+(3p^{-2}[1S]3d^2D)\text{Ar}$  are an exceptional case which does not fit in the picture presented above. Their ICD lifetimes are rather long (300 ÷ 1400 fs) and thus comparable to the characteristic time of vibrational motion (500 ÷ 1400 fs). However, since the minima of the corresponding PECs lie close to  $R_e$ , the effect of nuclear dynamics on the ICD spectra is rather small (see Fig. 5).

### C. Electronic and KER spectra

In this section, we present and discuss the total ICD electron and KER spectra of Ar dimer produced following the decay of the  $2p_{3/2} \rightarrow 4s$ ,  $2p_{1/2} \rightarrow 4s$ , and  $2p_{3/2} \rightarrow 3d$  parent core excitations of Ar. The resulting spectra are shown in Figs. 5 and 6. It can be seen from Fig. 5 that the electron spectra for all three parent excitations possess a double peak structure. The peak at lower energies (0 - 3 eV) originates mainly from the ICD of the four lowest ionization satellites:  $\text{Ar}^+(3p^{-2}[1S]4s^2S)\text{Ar}$ ,

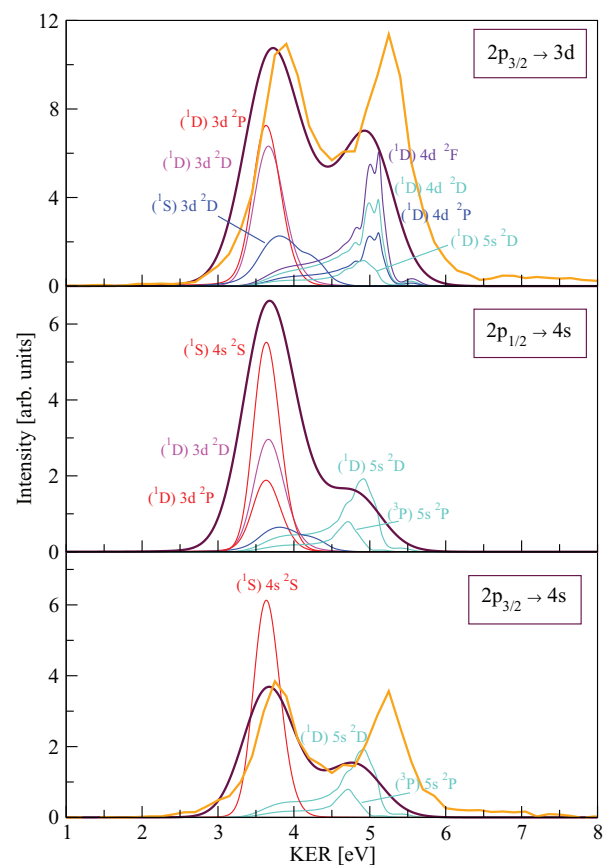


FIG. 6. KER spectra obtained in the RA-ICD cascade following the  $\text{Ar}(2p_{3/2} \rightarrow 4s)\text{Ar}$  (lowermost panel),  $\text{Ar}(2p_{1/2} \rightarrow 4s)\text{Ar}$  (middle panel), and  $\text{Ar}(2p_{3/2} \rightarrow 3d)\text{Ar}$  (uppermost panel) core excitation. The spectra were obtained using the mirror image principle (see Eq. (4)). The dark red curves in all panels represent the KER spectra corresponding to the particular core excitation. The orange lines are the experimental KER spectra for the  $\text{Ar}(2p_{3/2} \rightarrow 4s)\text{Ar}$  and  $\text{Ar}(2p_{3/2} \rightarrow 3d)\text{Ar}$  core excitation.<sup>14,50</sup> In order to compare the experimental spectra with the theoretical ones, the latter were convolved using a Gaussian of FWHM 0.64 eV and scaled so that the intensities of the lower-energy peaks coincide. The KER spectra of the satellites contributing to the total spectrum of each core excitation are also presented (the color scheme follows that of the PECs in Fig. 2).

$\text{Ar}^+(3p^{-2}[1D]3d^2P, 2D)\text{Ar}$ , and  $\text{Ar}^+(3p^{-2}[1S]3d^2D)\text{Ar}$ , populated in the strict spectator Auger transition. The second peak is located at energies between 3 and 6 eV. It is predominantly due to the ICD of the higher Rydberg states:  $\text{Ar}^+(3p^{-2}[3P]5s^2P)\text{Ar}$ ,  $\text{Ar}^+(3p^{-2}[1D]5s^2D)\text{Ar}$ ,  $\text{Ar}^+(3p^{-2}[1D]4d^2P, 2D, 2F)\text{Ar}$ , which are populated in a shake-up process during the resonant Auger step.<sup>18</sup> The relative intensities of the peaks reflect, therefore, the relative probability of shake-up processes in the RA decay of a particular parent state.

If one considers only the populations of the satellites decaying by ICD, the ratios of the strict spectator to shake-up probabilities for the  $2p_{3/2} \rightarrow 4s$ ,  $2p_{1/2} \rightarrow 4s$ , and  $2p_{3/2} \rightarrow 3d$  parent states are approximately 2:1, 3:1, and 1:1. This is clearly reflected in the resulting ICD electron spectra. The low energy peak dominates the high energy one for the  $2p_{3/2} \rightarrow 4s$  and  $2p_{1/2} \rightarrow 4s$  parent states and is more pronounced in the former case. Unlike these spectra, the two peaks in the electron spectrum of the  $2p_{3/2} \rightarrow 3d$  core excitation have

almost equal intensities, a result of a very large shake-up probability for this state.<sup>9,17</sup>

The KER spectrum carries information about the inter-nuclear distances at which ICD takes place and is, therefore, sensitive to the ratio of the electronic decay lifetime to the vibrational period. The Ar<sub>2</sub> spectra corresponding to the parent states in question are shown in Fig. 6. They possess a double-peak structure as the respective ICD electron spectra, although for a different physical reason. In the electron spectra, this structure reflects the differences in the populations and excitation energies of the satellite states following the resonant Auger decay, while in the KER spectra it is a sign that the ICD of different satellite states proceeds with notably different rates. In our previous analysis, we showed that lower Rydberg states decay fast with interatomic distances being close to  $R_e$ . This results in the peak located at energies between 2.5 and 4.5 eV. The longer ICD lifetimes of the higher Rydberg states lead to the decay close to the left turning point of the corresponding PECs, i.e. at shorter interatomic distances, resulting in the peak between 4.5 and 6 eV.

The computed ICD and KER spectra of the  $2p_{3/2} \rightarrow 4s$  and  $2p_{3/2} \rightarrow 3d$  parent states are in good agreement with the experimental results<sup>14,16,50</sup> as is evident from Figs. 5 and 6. Both electron and KER experimental spectra show the double-peak structure discussed above. There are, however, certain discrepancies in the positions of the computed and measured peaks. In particular, in the computed ICD electron spectrum corresponding to the Ar( $2p_{3/2} \rightarrow 3d$ )Ar parent core excited state the two peaks are shifted by 85 meV and 315 meV, respectively, to higher energies relative to the experimental spectrum. A shift of  $\sim 180$  meV to higher energies is clearly visible for the two peaks in the ICD electron spectrum corresponding to the Ar( $2p_{3/2} \rightarrow 4s$ )Ar parent excitation. Comparing the experimental and theoretical KER spectra, one sees that the theoretical spectrum is shifted to smaller energies of the emitted ionic fragments. In the case of the Ar( $2p_{3/2} \rightarrow 3d$ )Ar excitation, the shifts of the low and high Rydberg peaks are 170 meV and 320 meV, while for the Ar( $2p_{3/2} \rightarrow 4s$ )Ar excitation the respective shifts are 240 meV and 480 meV.

As one can see, from the total ICD electron spectra corresponding to all considered core-excited states (see Fig. 5) the peaks corresponding to the lower energy satellites are shifted less than the peaks corresponding to the higher energy ones. This is indicative of the different sources of error in the computation of the decay of the respective satellites. The KER spectra (see Fig. 6) show a similar behavior. However, due to energy conservation (see Eq. (4)), the shifts of the peaks have signs opposite to the shifts in the electron spectra.

For the fast decaying satellites, the resulting peaks in the ICD electron spectrum are sensitive to the quality of the ground state vibrational wave packet, relative populations of the satellite states in the RA decay and the energy difference between the decaying and final states close to the equilibrium distance  $R_e$ . It is clear from Fig. 3 (see also Ref. 37) that an error in the initial wave packet immediately translates into an error in the spectral peak. As we mentioned earlier, our ground state PEC compared to a benchmark computation

has a minimum shifted by 0.04 Å towards larger interatomic distances and also underestimates the binding by 0.8 meV. The combined effect would be to shift the maximum of the respective wave packet to larger interatomic distances shifting the electron peaks to larger energies by a few tens meV compared to the benchmark wave packet. The effect of the relative populations is relevant in the case of the Ar( $2p_{3/2} \rightarrow 3d$ )Ar parent excitation. The low-energy peak is composed of two peaks of nearly equal intensity arising due to ICD of the Ar<sup>+</sup>( $3p^{-2}[^1D]3d^2P, ^2D$ )Ar states (see Fig. 5). One can see that by changing the relative intensity of these constituent peaks one would shift the combined peak by at most 200 meV. However, as discussed at the end of Sec. II C, the atomic intensities we used in this work were experimentally shown to be accurate in the dimer. The errors in the energies of the decaying and the final states around  $R_e$  are less than 100 meV. A comparable value will be an upper boundary on their energy difference. One can see that the difference between the corresponding peaks in the theoretical and experimental spectra in Fig. 5 is a few tens meV agreeing well with the estimates made above.

The position of the low-energy peak in the KER spectrum originating from the lower Rydberg states depends on the quality of the ground state vibrational wave packet and the accuracy of the PECs of the final states around  $R_e$ . In the previous paragraph, we concluded that both errors will be below a hundred meV. The total observed shift is 170 meV which again agrees with our estimate (see Fig. 6).

The analysis of the computational errors in the case of the slow decaying satellites is much more complicated than in the case of the fast decaying ones. The accuracy in the positions of the corresponding peaks in both ICD electron and KER spectra is primarily determined by the accuracy of the positions of the left turning points on the PECs in question and the respective ICD rates. In Fig. 4, we show the electron spectrum corresponding to a slow decay from a single satellite state. It has a pronounced maximum at low energies corresponding to the decay around the left turning point and another maximum at higher energies due to the decay around the ground state equilibrium distance. Since the *ab initio* calculation of decay widths, especially for interatomic processes is difficult, one cannot expect the computed widths to be highly accurate (see Refs. 36, 51, and 52). A larger ICD rate leads to the reduction in the effect of nuclear dynamics, enhancing the spectrum in the higher-energy region. On the contrary, smaller ICD rate accentuates the effect of nuclear dynamics, enhancing the spectrum in the lower-energy part of the peak.<sup>51</sup> These errors may, therefore, produce a shift in the positions of the slow satellite peaks in the total electron and KER spectra. We also introduce an error in the turning point positions by modeling the higher satellite PECs with the PECs of the respective dicationic states. Although due to the diffuse nature of the Rydberg electron there is a good correspondence between the two types of PECs, the residual screening of the dicationic core by the Rydberg electron leads to differences in the slope of the repulsive part of the potentials.<sup>28</sup>

Finally, we would like to discuss briefly the effect of omitting some ICD states from the calculations (see Fig. 2 for the satellites in question, their PECs are shown in *grey*). The

largest deviation from the experiment should be observed for the ICD spectra of the  $2p_{3/2} \rightarrow 3d$  parent state where the neglected satellites carry up to 30% of the intensity. As can be seen from Fig. 2 these states form three groups lying in the energy ranges  $38 \div 39$  eV,  $40 \div 42$  eV, and above 42 eV, respectively. The decay of the states belonging to the first group would produce electrons with energies between 1.6 and 2.1 eV. The decay of the second group of states is expected to produce electrons of energies  $3.5 \div 4.2$  eV and, thus enhance the high-energy peak. The highest Rydberg states would decay emitting electrons of energies above 5 eV, which would account for the difference between the theoretical and experimental spectra in this region. All of the above mentioned states are slow decaying and would contribute to the high-energy peak in the KER spectrum.

#### IV. SUMMARY AND CONCLUSION

In this article, we present the results of *ab initio* computations of ICD electron and kinetic energy release spectra produced in the resonant-Auger - ICD cascades following  $2p_{3/2} \rightarrow 4s$ ,  $2p_{1/2} \rightarrow 4s$ , and  $2p_{3/2} \rightarrow 3d$  core excitations of Ar in Ar<sub>2</sub>. We computed the potential energy curves of the ionization satellites of Ar<sub>2</sub> populated in the resonant Auger steps, the repulsive two-site dicationic final states, as well as the ICD rates. These quantities were used to simulate quantum mechanically the nuclear dynamics during the decay and to derive the ICD spectra.

The computation of the decay rates revealed that the ionization satellites corresponding to the lowest terms of the respective Rydberg series have lifetimes between 28 and 130 fs. These lifetimes are considerably shorter than the characteristic vibrational periods of the satellites PECs. The lifetimes of the higher Rydberg states lie between 0.6 and 6.6 ps and are longer than the vibrational periods. Therefore, ICD of the former states is unaffected by nuclear dynamics; it proceeds around the Ar<sub>2</sub> equilibrium interatomic distance  $R_e$  and the resulting peaks in the spectra retain the shape of the initial vibrational wave packet. However, the dynamics play an important role in the decay of the higher satellites. Due to the larger ICD lifetimes the decay takes place mostly at interatomic distances close to the left turning points of the corresponding PECs. This shifts the positions of the peaks in the ICD electron spectra by about 1 eV to smaller energies than would be the case had the decay happened at  $R_e$ . The corresponding peaks in the KER spectra are shifted by about 1 eV towards higher energies due to energy conservation. The shapes of the resulting peaks strongly deviate from the shape of the initial vibrational wave packet.

The total ICD spectra exhibit a double-peak structure due to the population of higher Rydberg terms in the shake-up process during the resonant Auger step. The computed spectra deriving from the  $2p_{3/2} \rightarrow 4s$  and  $2p_{3/2} \rightarrow 3d$  excitations agree well with the available experimental results. The differences in the positions of the calculated and experimentally observed peaks are about a few hundred meV.

The total KER spectra also exhibit a double-peak structure. However, in this case the presence of two peaks indicates that there are two types of decaying states, which decay at

two different internuclear separations – the ground state equilibrium distance  $R_e$  and the left turning points of the corresponding PECs. The ICD electron and KER spectra of the individual ICD states were shown to be the mirror image of each other. Therefore, the shifts of the theoretical peaks in the total KER spectrum compared to the experimental ones are of the same order as those in the total ICD electron spectrum, but have the opposite sign.

The study of the impact of nuclear dynamics on ICD following resonant Auger gives insight into the mechanism of controlling the energies of the emitted electrons suggested recently.<sup>7</sup> Understanding the decay cascade in detail, in particular the origin of the different peaks in the spectra, can be used to predict the spectra of similar weakly bound diatomic systems (consisting of identical or different atoms) without explicitly calculating the nuclear dynamics during the decay. This allows for simulation of the spectra in a simple way where only knowledge of the decay rates at the ground state equilibrium distance, and the PECs of the decaying and final states is required. This may also be of importance in larger clusters, since for such systems it becomes computationally impossible to calculate the electron and KER spectra using nuclear dynamics.

#### ACKNOWLEDGMENTS

T.M. and K.G. would like to thank N. Sisourat, S. Klaiman, and T. Jahnke for the fruitful discussions. The authors are also grateful to K. Ueda and H. Fukuzawa for kindly providing us with their unpublished results and giving us permission to use them in our publication. We would like to acknowledge the use of the computing resources provided by bwGRiD (<http://www.bw-grid.de>), member of the German D-Grid initiative, funded by the Ministry for Education and Research (Bundesministerium für Bildung und Forschung) and the Ministry for Science, Research and Arts Baden-Wuerttemberg (Ministerium für Wissenschaft, Forschung und Kunst Baden-Württemberg). The work was supported by Research Unit 1789 (Interatomic Coulombic Decay) of the Deutsche Forschungsgemeinschaft. T.M. acknowledges the financial support of the HGS Mathcomp. P.K. acknowledges financial support from the Czech Science Foundation (Project No. GAČR P208/12/0521).

<sup>1</sup>A. Mozumder, *Fundamentals of Radiation Chemistry* (Academic Press, 1999).

<sup>2</sup>L. S. Cederbaum, J. Zobeley, and F. Tarantelli, *Phys. Rev. Lett.* **79**, 4778 (1997).

<sup>3</sup>U. Hergenhahn, *J. Electron Spectrosc. Relat. Phenom.* **184**, 78 (2011).

<sup>4</sup>W. Pokapanich, N. V. Kryzhevoi, N. Ottosson, S. Svensson, L. S. Cederbaum, G. Öhrwall, and O. Björneholm, *J. Am. Chem. Soc.* **133**, 13430 (2011).

<sup>5</sup>S. D. Stoychev, A. I. Kuleff, and L. S. Cederbaum, *J. Am. Chem. Soc.* **133**, 6817 (2011).

<sup>6</sup>N. V. Kryzhevoi and L. S. Cederbaum, *Angew. Chem., Int. Ed.* **50**, 1306 (2011).

<sup>7</sup>K. Gokhberg, P. Kolorenč, A. I. Kuleff, and L. S. Cederbaum, *Nature (London)* **505**, 661 (2014).

<sup>8</sup>K. Ueda, *J. Phys. Soc. Jpn.* **75**, 032001 (2006).

<sup>9</sup>H. Aksela, S. Aksela, and H. Pulkkinen, *Phys. Rev. A* **37**, 1798 (1988).

<sup>10</sup>T. W. Gorczyca and F. Robicheaux, *Phys. Rev. A* **60**, 1216 (1999).

<sup>11</sup>U. Hergenhahn, A. Rüdél, K. Maier, A. Bradshaw, R. Fink, and A. Wen, *Chem. Phys.* **289**, 57 (2003).

- <sup>12</sup>P. Bolognesi, P. O'Keefe, Y. Ovcharenko, M. Coreno, L. Avaldi, V. Feyer, O. Plekan, K. C. Prince, W. Zhang, and V. Carravetta, *J. Chem. Phys.* **133**, 034302 (2010).
- <sup>13</sup>F. Trinter, M. S. Schöffler, H.-K. Kim, F. P. Sturm, K. Cole, N. Neumann, A. Vredenberg, J. Williams, I. Bocharova, R. Guillemin *et al.*, *Nature (London)* **505**, 664 (2014).
- <sup>14</sup>M. Kimura, H. Fukuzawa, K. Sakai, S. Mondal, E. Kukk, Y. Kono, S. Nagaoka, Y. Tamenori, N. Saito, and K. Ueda, *Phys. Rev. A* **87**, 043414 (2013).
- <sup>15</sup>P. O'Keefe, E. Ripani, P. Bolognesi, M. Coreno, M. Devetta, C. Callegari, M. Di Fraia, K. C. Prince, R. Richter, M. Alagia *et al.*, *J. Phys. Chem. Lett.* **4**, 1797 (2013).
- <sup>16</sup>M. Kimura, H. Fukuzawa, T. Tachibana, Y. Ito, S. Mondal, M. Okunishi, M. Schöffler, J. Williams, Y. Jiang, Y. Tamenori *et al.*, *J. Phys. Chem. Lett.* **4**, 1838 (2013).
- <sup>17</sup>M. Meyer, E. v. Raven, B. Sonntag, and J. Hansen, *Phys. Rev. A* **43**, 177 (1991).
- <sup>18</sup>J. A. de Gouw, J. van Eck, A. C. Peters, J. van der Weg, and H. G. M. Heideman, *J. Phys. B: At. Mol. Opt. Phys.* **28**, 2127 (1995).
- <sup>19</sup>J. C. Fuggle and S. F. Alvarado, *Phys. Rev. A* **22**, 1615 (1980).
- <sup>20</sup>P. Piecuch, S. A. Kucharski, K. Kowalski, and M. Musiał, *Comput. Phys. Commun.* **149**, 71 (2002).
- <sup>21</sup>K. Raghavachari, G. W. Trucks, J. A. Pople, and M. Head-Gordon, *Chem. Phys. Lett.* **157**, 479 (1989).
- <sup>22</sup>T. Van Mourik and T. H. Dunning, *Int. J. Quantum Chem.* **76**, 205 (2000).
- <sup>23</sup>P. R. Herman, P. E. Larocque, and B. P. Stoicheff, *J. Chem. Phys.* **89**, 4535 (1988).
- <sup>24</sup>B. R. Brooks and H. F. Schaefer, *J. Chem. Phys.* **70**, 5092 (1979).
- <sup>25</sup>B. R. Brooks, W. D. Laidig, P. Saxe, N. C. Handy, and H. F. Schaefer III, *Phys. Scr.* **21**, 312 (1980).
- <sup>26</sup>D. E. Woon and T. H. Dunning, Jr., *J. Chem. Phys.* **98**, 1358 (1993).
- <sup>27</sup>The exponents of the diffuse *s* functions are 0.0739 and 0.0234. The exponents of the *d* functions are: 2.3300 and 7.3800 for the two compact *d* functions, and 0.2330 and 0.0738 for the two diffuse *d* functions.
- <sup>28</sup>T. Miteva, S. Klaiman, E. V. Gromov, and K. Gokhberg, *J. Chem. Phys.* **140**, 204320 (2014).
- <sup>29</sup>A. Kramida, Y. Ralchenko, J. Reader, and N. A. Team, NIST Atomic Spectra Database (version 5.1) (National Institute of Standards and Technology, Gaithersburg, MD 2013), see <http://physics.nist.gov/asd>.
- <sup>30</sup>V. Averbukh and L. S. Cederbaum, *J. Chem. Phys.* **123**, 204107 (2005).
- <sup>31</sup>A. Nicklass, M. Dolg, H. Stoll, and H. Preuss, *J. Chem. Phys.* **102**, 8942 (1995).
- <sup>32</sup>K. Kaufmann, W. Baumeister, and M. Jungen, *J. Phys. B: At. Mol. Opt.* **22**, 2223 (1989).
- <sup>33</sup>V. Averbukh, I. B. Müller, and L. S. Cederbaum, *Phys. Rev. Lett.* **93**, 263002 (2004).
- <sup>34</sup>S. Scheit, L. S. Cederbaum, and H.-D. Meyer, *J. Chem. Phys.* **118**, 2092 (2003).
- <sup>35</sup>S. Scheit, V. Averbukh, H.-D. Meyer, N. Moiseyev, R. Santra, T. Sommerfeld, J. Zobeley, and L. S. Cederbaum, *J. Chem. Phys.* **121**, 8393 (2004).
- <sup>36</sup>P. V. Demekhin, S. Scheit, S. D. Stoychev, and L. S. Cederbaum, *Phys. Rev. A* **78**, 043421 (2008).
- <sup>37</sup>P. V. Demekhin, Y.-C. Chiang, S. D. Stoychev, P. Kolorenč, S. Scheit, A. I. Kuleff, F. Tarantelli, and L. S. Cederbaum, *J. Chem. Phys.* **131**, 104303 (2009).
- <sup>38</sup>E. Pahl, H.-D. Meyer, and L. S. Cederbaum, *Z. Phys. D* **38**, 215 (1996).
- <sup>39</sup>T. F. O'Malley, *Phys. Rev.* **150**, 14 (1966).
- <sup>40</sup>J. N. Bardsley, *J. Phys. B At. Mol. Opt. Phys.* **1**, 349 (1968).
- <sup>41</sup>L. S. Cederbaum and W. Domcke, *J. Phys. B At. Mol. Opt. Phys.* **14**, 4665 (1981).
- <sup>42</sup>W. T. Pollard and R. A. Friesner, *J. Chem. Phys.* **100**, 5054 (1994).
- <sup>43</sup>H.-D. Meyer, U. Manthe, and L. S. Cederbaum, *Chem. Phys. Lett.* **165**, 73 (1990).
- <sup>44</sup>H.-D. Meyer, G. A. Worth, M. H. Beck, A. Jäckle, U. Manthe, M. Ehara, A. Raab, M.-C. Heitz, S. Sukiasyan, C. Cattarius *et al.*, The MCTDH Package, version 8.4 (2007), see <http://mctdh.uni-hd.de/>.
- <sup>45</sup>N. Moiseyev, R. Santra, J. Zobeley, and L. S. Cederbaum, *J. Chem. Phys.* **114**, 7351 (2001).
- <sup>46</sup>T. Jahnke, A. Czasch, M. S. Schöffler, S. Schössler, A. Knapp, M. Käs, J. Titze, C. Wimmer, K. Kreidi, R. E. Grisenti *et al.*, *Phys. Rev. Lett.* **93**, 163401 (2004).
- <sup>47</sup>Y.-C. Chiang, F. Otto, H.-D. Meyer, and L. S. Cederbaum, *J. Chem. Phys.* **136**, 114111 (2012).
- <sup>48</sup>F. Trinter, J. B. Williams, M. Weller, M. Waitz, M. Pitzer, J. Voigtsberger, C. Schober, G. Kastirke, C. Müller, C. Gohl *et al.*, *Phys. Rev. Lett.* **111**, 093401 (2013).
- <sup>49</sup>N. Sisourat, N. V. Kryzhevoi, P. Kolorenč, S. Scheit, T. Jahnke, and L. S. Cederbaum, *Nat. Phys.* **6**, 508 (2010).
- <sup>50</sup>K. Ueda and H. Fukuzawa, private communication (2014).
- <sup>51</sup>T. Ouchi, K. Sakai, H. Fukuzawa, I. Higuchi, P. V. Demekhin, Y.-C. Chiang, S. D. Stoychev, A. I. Kuleff, T. Mazza, M. Schöffler *et al.*, *Phys. Rev. A* **83**, 053415 (2011).
- <sup>52</sup>G. Jabbari, S. Klaiman, Y.-C. Chiang, F. Trinter, T. Jahnke, and K. Gokhberg, *J. Chem. Phys.* **140**, 224305 (2014).